Impedance spectroscopy analysis of small molecule solution processed organic solar cell

B. Arredondo [a,*], B. Romero [a], G. Del Pozo [a], M. Sessler [b,c], C. Veit [b], U. Würfel [b,c]

[a] Dpto. Tecnología Electrónica, Universidad Rey Juan Carlos, C/ Tulipán s/n, 28933 Móstoles, Madrid, Spain
[b] Fraunhofer Institute for Solar Energy Systems ISE, Heidenhofstr. 2, 79110 Freiburg, Germany
[c] Freiburg Materials Research Center, FMF, Stefan-Meier-Str. 21, 79104 Freiburg, Germany

ARTICLE INFO

ABSTRACT

In this paper we study the transport-recombination mechanisms using impedance spectroscopy of organic solar cells (OSC) based on a blend of a small molecule, 7,7′-(4,4-bis(2ethylhexyl)-4H-silolo[3,2-b:4,5-b′] dithiophene-2,6-diyl)bis(6-fluoro-4-(5′-hexyl-[2,2′-bithiophen]-5-yl)benzo[c][1,2,5] thiadiazole) (DTS(FBTTh$_2$)$_2$) and 1-(3-methoxycarbonyl)-propyl-1-1-phenyl-(6,6) C70 (PC$_{70}$BM). We fabricate a cell with structure ITO/Poly(3,4-ethylenedioxythiophene)-poly(4-styrene sulfonate (PEDOT:PSS))/DTS (FBTTh$_2$)$_2$:PC$_{70}$BM/Ca/Al that exhibits $J_{sc}=10.2$ mA/cm^2, $V_{oc}=0.816$ V and FF$=65\%$ resulting in a PCE$=5.4\%$. We model the impedance behavior using two circuital models, the parallel R-CPE and the transmission line model proposed by Belmonte et al. [1]. We compared the results to those obtained for OSC based on a standard poly(3-hexylthiophene) (P3HT): 1-(3-methoxycarbonyl)-propyl-1-1-phenyl-(6,6) C61 (PC$_{60}$BM) blend with structure ITO/PEDOT:PSS/P3HT:PC$_{60}$BM/LiF/Al. We find that in the case of the small molecule based OSC diffusion dominates over recombination for this thickness, $L=125$ nm, even at high frequencies. We calculate the effective carrier lifetimes and mobilities for both structures using both models. Average electron mobility calculated for the small molecule cell is around 4–6.4×10^{-3} cm^2/Vs, slightly higher than that obtained for the standard blend which is around 2×10^{-3} cm^2/Vs.

© 2014 Elsevier B.V. All rights reserved.

1. Introduction

Bulk-heterojunction (BHJ) organic solar cells (OSC) have the potential to become real alternative to silicon-based devices due to the advantages they offer: lightness, thinness and potential flexibility [2,3]. Besides, the active layer material is solution processable, allowing low-cost fabrication techniques such as spin coating for small areas and different printing techniques in a continuous Roll-to-Roll process for large areas [4–6]. Although blends of conjugated polymers and fullerene derivatives have been one of the most popular due to the high efficiencies achieved [7] recently, devices based on blends of small molecules and fullerene derivatives have achieved high efficiencies, up to 9% [8]. As donor materials, small molecules offer additional advantages over polymers: the molecular structure is better defined and therefore the molecular weight and the material purity have low variations from batch to batch or among different materials supplier companies. Besides, in small molecules chemical properties can be finer tuned

which also results in a better tuning of optical, electronic and physical characteristics.

Impedance Spectroscopy (IS) has been successfully used both in inorganic [9,10] and OSC to obtain valuable information about kinetics and energetic processes governing the device performance [11]. It is also a valuable tool to observe bulk and interfacial electrical properties that cannot be observed in direct current regime [12]. This technique consists in applying a small sinusoidal voltage superimposed on a bias voltage. By fitting the frequency response of the electrical impedance to a circuit model, information about cell resistances and capacitances can be extracted. In the literature different equivalent circuit models have been proposed to simulate the impedance of OSC: i) the simple parallel RC model, which results in perfect semicircular Cole–Cole diagrams, ii) the parallel R-CPE model used in [13–15], that results in depressed circular diagrams. This circuit includes an extra fitting parameter to model non ideal non-homogeneities such as porosities, roughness and surface states iii) The Mani parallel model [16] which consist in a parallel R$_1$CPE$_1$ in parallel with a series combination of R$_2$ and a second constant phase element, CPE$_2$ iv) Belmonte transmission line model, which includes distributed transport resistors, R_t, standing for carrier transport, and a distributed chemical capacitance, C_μ, in parallel with a recombination

resistance, R_{rec} [1,17]. Impedance spectroscopy allows the determination of different electronic parameters, such as the built-in voltage, the doping concentration, the effective recombination lifetime and the diffusion time. From the diffusion time, diffusion coefficient and carrier mobility can be obtained [12,15,1]. Some authors have also used this technique to obtain the electron and hole carrier density and the density of states function [11].

In this paper we present a study of OSCs based on two different blends, the standard P3HT:PC$_{60}$BM and a new blend that uses a small molecule as donor material, pDTS(FBTTh$_2$)$_2$:PC$_{70}$BM. The layer structure is ITO/PEDOT:PSS/P3HT: PC$_{60}$BM/LiF/Al and ITO/PEDOT:PSS/pDTS(FBTTh$_2$)$_2$:PC$_{70}$BM/Ca/Al, respectively. Cells have been optimized in terms of efficiency by adjusting some fabrication parameters such as ratio, concentration, annealing conditions, etc. Current density–voltage (J–V) curves are given and cell performance parameters are compared. Impedance spectra have been measured in dark at different bias voltages, and under varying illumination densities (at open circuit conditions, V_{OC}). Impedance data have been fitted with two models (the parallel RCPE and the transmission line model) and the extracted circuital parameters have been related to the transport processes occurring in the organic semiconductor.

2. Experimental details

2.1. OSC fabrication

Commercial ITO coated glass substrates (Präzisions Glas & Optik GmbH, 25 mm × 25 mm) were first manually washed in aqueous detergent and then sonicated for 10 min twice in acetone, isopropanol and de-ionised water. Substrates were blow dried with nitrogen and treated with UV ozone for 20 minutes.

PEDOT:PSS suspension (Clevios P VP Al4083) was filtered (with 0.45 mm PVDF filter), spin coated at 3.000 rpm for 60 s and annealed on a hot plate at 130 °C for 10 min yielding a thickness of 35 nm. The active layer blend of DTS(FBTTh$_2$)$_2$:PCB$_{70}$M (P3HT: PC$_{60}$BM) was spin coated and annealed on a hot plate at 150 °C yielding an active layer thickness of 125 nm (220 nm). Finally, a thin layer of 20 nm Ca (0.5 nm LiF) followed by a layer of Al (100 nm) were thermally evaporated on top of the device with a vacuum pressure lower than 10^{-5} mbar.

2.2. OSC characterization

J-V curves were measured using a Keithley 2400 Sourcemeter and a Steuernagel SolarCellTest 575 sun-simulator. Impedance spectra were measured using an IM6 Electrochemical Workstation from Zahner-elektrik. Samples were measured inside a flow cell, where a constant nitrogen flow was set in order to avoid degradation. A halogen lamp was used for illumination. Impedance spectra were recorded by applying a small voltage perturbation (20 mV rms) at frequencies from 1 MHz to 1 Hz in dark conditions (for voltages varying from −3 to 1 V). Illumination measurements were performed varying the irradiation intensity up to one sun (i.e., simulated AM 1.5 G, 1000 W/m^2), under open-circuit conditions.

3. Results and discussion

Fig. 1 shows the device layer sequence together with the molecular structure and the energy levels schematic. LUMO and HOMO levels of p-DTS(FBTTh$_2$)$_2$ have been reported by Poll et al. [18] using cyclic voltammetry and optical measurements. The difference between the HOMO level of donor molecule and
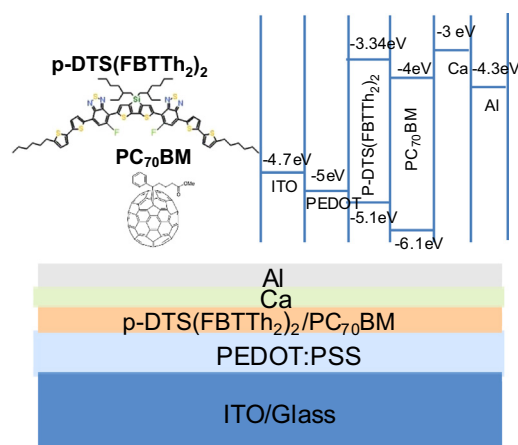

Fig. 1. Molecular structure, energy level diagram and device layer sequence.
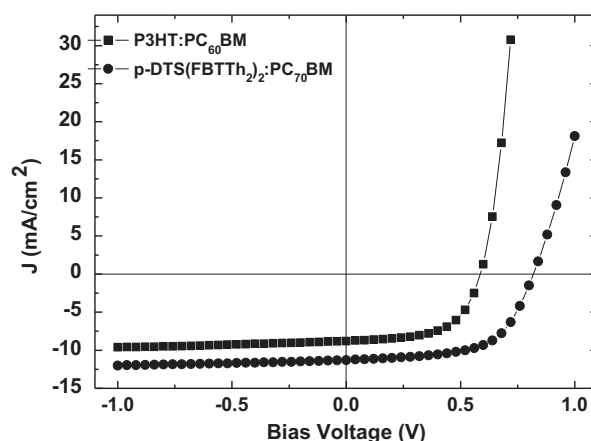

Fig. 2. J–V characteristic of the p-DTS(FBTTh$_2$)$_2$:PC$_{70}$BM and P3HT:PC$_{60}$BM solar cells under simulated AM1.5G (100 mW/cm^2) irradiance.

the LUMO level of the acceptor (fullerene derivative) is related to the cell V_{oc} [19,20]. Previous results show that this photoactive blend p-DTS(FBTTh$_2$)$_2$:PC$_{70}$BM leads to high values of V_{oc} ranging between 0.77–0.81 V and thus resulting in an improved PCE of up to 7% [18,8].

Fig. 2 shows the J–V characteristic of the bulk heterojunction small molecule solar cell under simulated AM1.5G irradiation (100 mW/cm^2). This solar cell exhibits J_{sc}=10.2 mA/cm^2, V_{oc}=0.816 V and FF=65% resulting in a PCE=5.4%. For the sake of comparison, Fig. 2 also displays the J–V of a standard P3HT:PC$_{60}$BM with similar layer structure both fabricated and measured under the same conditions. This standard cell exhibits J_{sc}=8.8 mA/cm^2, V_{oc}=0.574 V and FF=62%, leading to PCE=3.2%.

Fig. 3 shows the impedance spectra in dark conditions from 1 Hz up to 1 MHz for the small molecule solar cell at different bias voltages. Experimental data resemble the typical semicircle shape that can be accurately modeled with a simple parallel RC circuit. Solid lines show the fit. The capacitance C extracted from the fit is attributed to the depletion region capacitance due to the band bending at the contact [1]. This capacitance follows a voltage dependence according to the Mott–Schottky expression,

$$C^{-2} = \frac{2(V_{bi} - V)}{A^2 e \varepsilon \varepsilon_0 N_A} \tag{1}$$

where V_{bi} is the built-in potential, N_A is the acceptor impurity density, A is the area (=0.09 cm^2), V the applied voltage and ε and ε_0 are the dielectric constant and vacuum permittivity
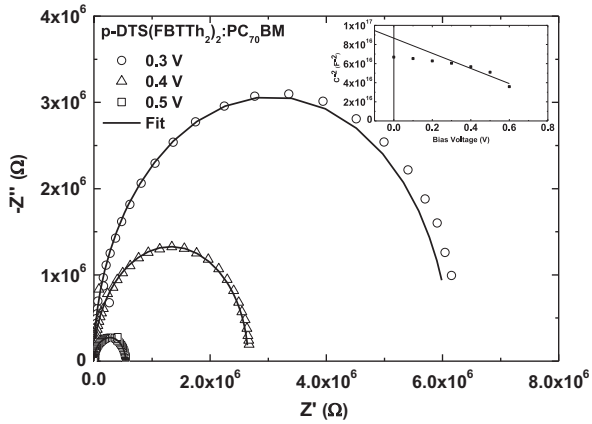
Fig. 3. Impedance spectra under dark conditions at different voltages. Solid lines show the fit to a parallel RC circuit. Inset shows C^{-2} vs V resembling typical Mott–Schottky behavior.

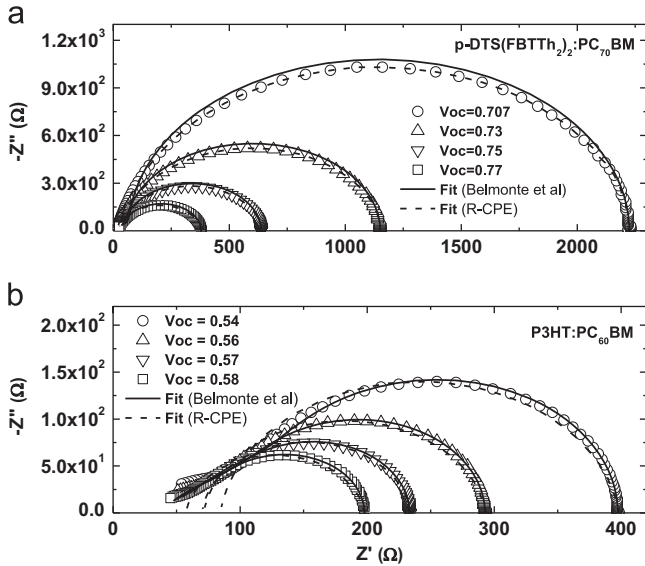**Fig. 4.** Open symbols show the impedance spectra measured under different irradiation intensities at open circuit conditions. (a) p-DTS(FBTTh$_2$)$_2$:PC$_{70}$BM based solar cell and (b) P3HT:PC$_{60}$BM based solar cell. Solid lines show the fit using the transmission line model proposed by García Belmonte et al. [1,17]. Dashed lines show the fit using the standard parallel R-CPE circuit.

respectively. The dielectric constant is estimated from the geometrical capacitance ($\varepsilon = CL/A\varepsilon_0$) at negative voltages leading to $\varepsilon = 5.3$, considerably larger than the value 3.6 obtained for the P3HT:PC$_{60}$BM

blend. The same dielectric constant values for both blends were obtained experimentally using the CELIV technique [21]. The built-in potential and the acceptor density have been obtained respectively from the intercept with the x-axis and the slope of the straight line shown in the inset in Fig. 3, leading to $V_{bi} = 1.09$ V and $N_A = 4.1 \times 10^{16}$ cm^{-3}. This built-in voltage, that refers to the cathode interface, is larger than that obtained for standard P3HT:PC$_{60}$BM solar cells of 0.45 V, similar to the one found by other authors [15,1].

Fig. 4 shows the impedance spectra measured under different irradiation intensities at open circuit conditions as explained in the experimental section. As expected, open circuit voltage increases with the irradiation intensity as indicated in the legend. The complex impedance plot of the small molecule cell resembles

a depressed semicircle, a classical behavior of BHJ solar cells, see Fig. 4(a). In the case of the P3HT:PC$_{60}$BM cell, the Cole–Cole plot shows two distinct regions: a large semicircle at low frequencies associated to the carrier recombination process, and a quasi straight line (with slope approximating to one) in the high frequency region containing information about the diffusion mechanism, see Fig. 4(b). This latter impedance behavior, associated to diffusion-recombination transport, is commonly obtained by several authors for this standard blend [12,1,22]. García Belmonte et al. have successfully modeled it using a transmission line circuit [9,12,1,17]. They model the diffusion mechanism at high frequencies using a transport resistance R_t and the recombination process at low frequencies through a recombination resistance R_{rec}. Diffusion and recombination times are defined as $\tau_d = C_\mu R_t$ and $\tau_n = C_\mu R_{rec}$ respectively, where C_μ is the chemical capacitance associated to the excess of carriers in the active layer. In particular, the chemical capacitance is related to the increase of the electrons occupancy in the fullerene LUMO [11,17]. They proposed an analytical solution for the impedance given by [17].

$$Z = \left(\frac{R_t R_{rec}}{1 + (i\omega/\omega_{rec})} \right)^{1/2} \coth\left[\left(\frac{\omega_{rec}}{\omega_d} \right)^{1/2} \left(1 + \frac{i\omega}{\omega_{rec}} \right)^{1/2} \right] \quad (2)$$

where ω is the angular frequency and, $\omega_d = 1/C_\mu R_t$ and $\omega_{rec} = 1/C_\mu R_{rec}$ are the diffusion and recombination frequencies, respectively.

In this work, experimental impedance data of P3HT:PC$_{60}$BM and p-DTS(FBTTh$_2$)$_2$:PC$_{70}$BM cells have been modeled using two electronic circuits, a classical parallel R-CPE circuit and the transmission line circuit proposed by García Belmonte et al. Dashed lines in Fig. 4 correspond to the impedance fit using a typical parallel R-CPE circuit where CPE is a non-ideal capacitance taking into account non-homogeneities such as porosities, roughness and surface states with $Z_{CPE} = 1/(CPE_T)(i\omega)^{(CPE_P)}$. Theoretically, CPE$_P$ values range from -1 (pure inductor) to 1 (pure capacitor). Most of our simulations result in CPE$_P$ ranging from 0.95 up to 1, thus approximating CPE to a capacitor with CPE$_T$ being the capacitance value. As expected, this circuit, similar to a parallel RC, cannot simulate the diffusion mechanism at high frequencies as can be clearly seen for the P3HT:PC$_{60}$BM cell in Fig. 4(b). Solid lines show that this diffusion behavior is well simulated by the transmission line model given by Eq. (2). In the case of the p-DTS (FBTTh$_2$)$_2$:PC$_{70}$BM cell, the diffusion mechanism at high frequencies is not that obvious. However, the Cole–Cole is not a symmetric semicircle with the slope at high frequencies being less than half of its value at low frequencies.

Systematic fits with both circuits at different bias agree well with experimental data in the low frequency part of the spectra and thus results in similar parameters associated to the recombination mechanism, R_{rec} and R_p (parallel resistance in the R-CPE circuit), see Fig. 5(a) and (b). Small molecule solar cells present a R_t one order of magnitude lower than those resistances associated to recombination (except for high bias). This indicates low recombination conditions, that is, diffusion dominates over recombination, at least for this thickness ($L = 125$ nm). In the ideal case where R_t vanishes, impedance will tend to a perfect semicircle modeled with a parallel pure RC. In this case, the diffusion time $\tau_d = C_\mu R_t$ will also vanish, meaning that carrier transport does not limit the cell performance. Only at high voltage (around 0.8 V and under one sun illumination), recombination begins to affect transport.

In the case of P3HT:PC$_{60}$BM based cells with $L = 220$ nm, R_t has similar value to R_{rec}, meaning that recombination is limiting carrier transport. This agrees with the Cole–Cole diagram of Fig. 4(b) showing diffusion behavior at high (but non-infinite)
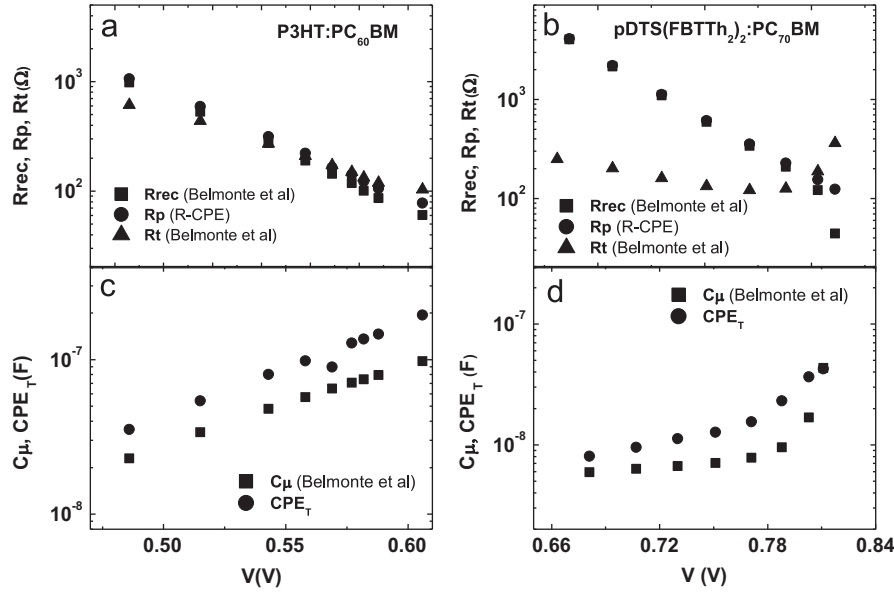
Fig. 5. Circuital parameters extracted from fits using two models, parallel R-CPE circuit and transmission line model (Belmonte et al.). Resistance and capacitance parameters of P3HT:PC$_{60}$BM solar cells (a) and (c), and pDTS(FBTTh$_2$)$_2$:PC$_{70}$BM solar cells (b) and (d).

frequency. It is worth mentioning that thicknesses in both cells were optimized in order to maximize solar cell efficiency.

Fig. 5(c) and (d) show that the chemical capacitance and the capacitance associated to the CPE circuit have values in the same order of magnitude and follow the same trend with bias voltage.

The J–V characteristic of a solar cell can be expressed as [17,23],

$$j = j_0\left[\exp\left(\beta\frac{V_F}{k_BT/q}\right) - 1\right] - j_{ph} \tag{3}$$

where j_0 is the saturation current, j_{ph} stands for the photocurrent, V_F is the applied voltage, and β is the inverse of the diode ideality factor. The first term in Eq. (3) is identified as the recombination current by Belmonte et al. This current can be assimilated to the typical voltage dependent current flowing throw the diode,

$$j_{rec} = j_0\left[\exp\left(\beta\frac{V_F}{k_BT/q}\right) - 1\right] \tag{4}$$

It is worth mentioning that j_{rec} is light independent while j_{ph} is voltage independent. j_{rec} can be obtained as function of the recombination resistance R_{rec} extracted from the fit of the impedance measurements. R_{rec} is the inverse of the derivative of the j_{rec} with respect to V_F,

$$R_{rec} = \left[\frac{dj_{rec}}{dV_F}\right]^{-1} \tag{5}$$

Differentiating Eq. (4) with respect to V_F, we obtain,

$$\frac{dj_{rec}}{dV_F} = j_0\beta\frac{q}{kT}\exp\left(\beta\frac{V_F}{k_BT/q}\right) = \beta\frac{q}{kT}j_{rec} \tag{6}$$

We can readily obtain an expression of j_{rec} as function of R_{rec},

$$j_{rec} = \frac{kT}{q\beta}\frac{dj_{rec}}{dV_F} = \frac{kT}{q\beta R_{rec}} \tag{7}$$

Fig. 6(a) and (b) shows the carrier lifetime using the extracted parameters from the impedance fit defined as $\tau_n = C_\mu R_{rec}$ at different voltages. Similar results were obtained using both circuital models, with lifetimes decreasing with bias and varying in the order of 10^{-5} s for both devices. Since all measurements were

carried out at open circuit conditions (J=0), Eq. (3) becomes,

$$j_{ph} = j_0\left[\exp\left(\beta\frac{V_F}{k_BT/q}\right) - 1\right] = j_{rec} \tag{8}$$

Fig. 6(c) and (d) shows the reconstructed $I_{rec} = A \cdot j_{rec}$ (with A=9.2 mm^2) applying Eq. (7) and using the recombination and parallel resistances extracted from the transmission line and R-CPE models respectively. Recombination current is in good agreement with the measured $I_{sc}(\approx I_{ph})$ at every bias as expected from Eq. (8). In the case of the small molecule devices, the reconstructed I_{rec} using the resistance from the R-CPE model at high bias deviates from the measured I_{sc}. This is attributed to the fact that at those biases recombination mechanism begin to limit transport as can be deduced from the increase of R_t (see Fig. 5(b)). In fact, in this regime, the R-CPE model differs in the complex impedance plot from the ideal semicircle given by a RC element since CPE$_P$ < 0.9.

Mobility of minority carriers can be obtained as

$$\mu_n = \frac{eL^2}{\tau_d kT} \tag{9}$$

where L is the active layer thickness and τ_d is the diffusion time. Fig. 7 shows the obtained mobility calculated using Eq. (9) with diffusion times obtained from the circuital parameters. The mobility values obtained for P3HT:PC$_{60}$BM are similar to those obtained by other authors in similar structures by means of impedance spectroscopy [1,15]. Although some authors relate a high short circuit current with high mobilities [24], in this case we believe that increased J_{sc} of the small molecule cell is simple caused by its broader absorption.

4. Conclusions

In summary we have investigated for the first time the conduction mechanisms and properties of a solar cell based on a small molecule pDTS(FBTTh$_2$)$_2$:PC$_{70}$BM blend using impedance spectroscopy. We obtained a built-in potential and an acceptor density of V_{bi}=1.09 V and N_A=4.1 × 10^{16} cm^{-3} respectively from the fit of the dark impedance data using a parallel RC circuit. We used two circuital models to fit the impedance data under varying illumination at V_{oc}, the parallel R-CPE circuit and transmission line
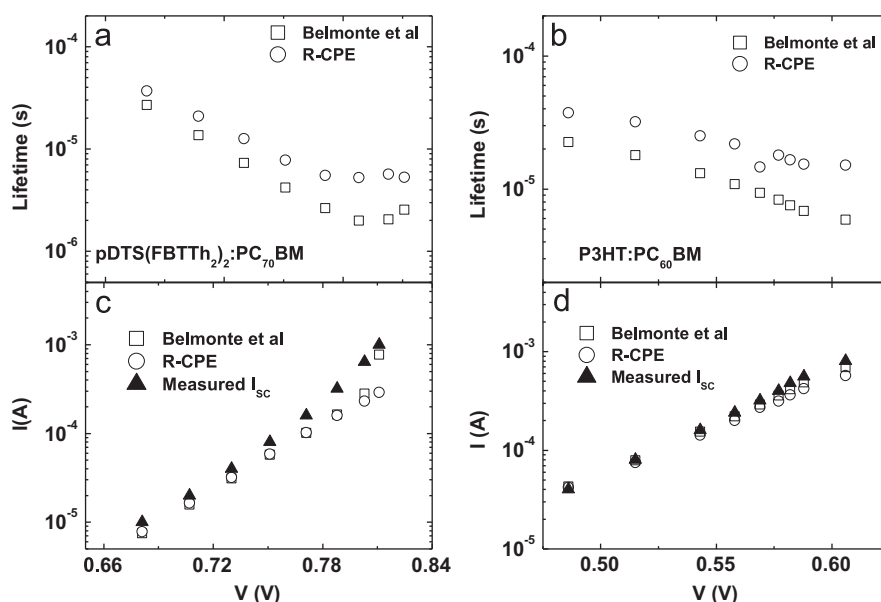
Fig. 6. Lifetimes calculated using the extracted parameters from the impedance fit (a) pDTS(FBTTh$_2$)$_2$:PC$_{70}$BM solar cells, and (b) P3HT:PC$_{60}$BM solar cells. Reconstructed recombination current using Eq. (7) and measured I$_{SC}$ of (c) pDTS(FBTTh$_2$)$_2$:PC$_{70}$BM solar cells, and (d) P3HT:PC$_{60}$BM solar cells.
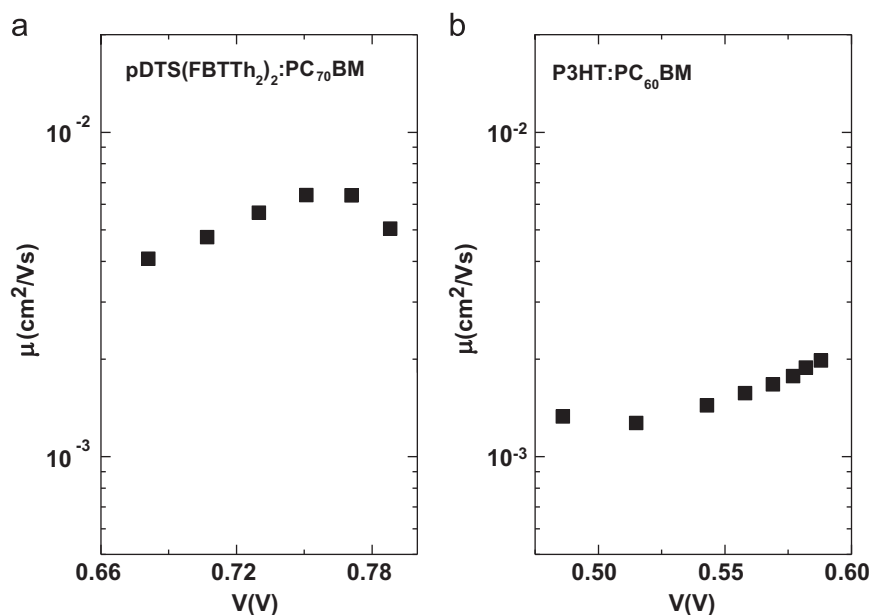
Fig. 7. Calculated mobility of (a) pDTS(FBTTh$_2$)$_2$:PC$_{70}$BM solar cells, and (b) P3HT:PC$_{60}$BM solar cells.

circuit proposed by Belmonte et al., and compared the results with those obtained for a standard cell based on a P3HT:PC$_{60}$BM blend. We extracted the circuital parameters and find that R_t for the small molecule is one order of magnitude lower than those resistances associated to recombination indicating low recombination conditions even at high frequencies (at least for this thickness). Only at very high voltages recombination begins to limit transport. We have also reconstructed the recombination current using the R_{rec} and R_p extracted from the fit of the impedance data under illumination and open circuit conditions to confirm that agrees well with the measured short circuit current. Mobilities are calculated from the diffusion times obtaining slightly higher values for the small molecule cells in order of 4–6.4×10^{-3} cm^2/Vs and 2×10^{-3} cm^2/Vs for the standard P3HT:PC$_{60}$BM blend.

Acknowledgments

References

[1] G. García-Belmonte, A. Munar, E.M. Barea, J. Bisquert, I. Ugarte, R. Pacios, Charge carrier mobility and lifetime of organic bulk heterojunctions analyzed by impedance spectroscopy, Org. Electron. 9 (2008) 847–851.
[2] C.J. Brabec, N.S. Sariciftci, J.C. Hummelen, Plastic solar cells, Adv. Mater. 11 (2001) 15–26.

[3] S.H. Park, A. Roy, S. Beaupré, S. Cho, N. Coates, J.S. Moon, D. Moses, M. Leclerc, K. Lee, A.J. Heeger, Bulk heterojunction solar cells with internal quantum efficiency approaching 100%, Nat. Photonis 3 (2009) 297–302.

[4] C.N. Hoth, S.A. Choulis, P. Schilinsky, C.J. Brabec, On the effect of poly(3-hexylthiophene) regioregularity on inkjet printed organic solar cells, J. Mater. Chem. 19 (2009) 5398–5404.

[5] F.C. Krebs, All solution roll-to-roll processed polymer solar cells free from indium-tin-oxide and vacuum coating steps, Org. Electron. 10 (2009) 761–768.

[6] F.C. Krebs, Fabrication and processing of polymer solar cells: a review of printing and coating techniques, Sol. Energy Mat. Sol. Cells 93 (2009) 394–412.

[7] S.H. Lee, J.H. Kim, T.H. Shim, J.G. Park, Effect of interface thickness on power conversion efficiency of polymer photovoltaic cells, Electron. Mater. Lett. 5 (2009) 47–50.

[8] V. Gupta, A.K.K. Kyaw, D.H. Wang, S. Chand, G.C. Bazan, A.J. Heeger, Barium: an efficient cathode layer for bulk-heterojunction solar cells, Nat. Sci. Rep. 3 (2013) 1965.

[9] I. Mora-Seró, G. García-Belmonte, P.P. Boix, M.A. Váquez, J. Bisquert, Impedance spectroscopy characterisation of highly efficient silicon solar cells under different light illumination intensities, Energy Environ. Sci. 2 (2009) 678–686.

[10] R.A. Kumar, M.S. Suresh, J. Nagaraju, Measurement and comparison of AC parameters of silicon (BSR and BSFR) and gallium arsenide (GaAs/Ge) solar cells used in space applications, Sol. Energy Mater. Sol. Cells 60 (2000) 155–166.

[11] G. García-Belmonte, P.P. Boix, J. Bisquert, M. Sesolo, H.J. Bolink, Simultaneous determination of carrier lifetime and electron density-of-states in P3HT:PCBM organic solar cells under illumination by impedance spectroscopy, Sol. Energy Mater. Sol. Cells 94 (2010) 366–375.

[12] T. Ripolles-Sanchís, A. Guerrero, J. Bisquert, G. García-Belmonte, Diffusion-recombination determines collected current and voltage in polymer: fullerene solar cells, J. Phys. Chem. C 116 (2012) 16925–16933.

[13] T. Kuwabara, C. Iwata, T. Yamaguchi, K. Takahashi, Mechanistic insights into UV-induced electron transfer from PCBM to titanium oxide in inverted-type organic thin film solar cells using AC impedance spectroscopy, Appl. Mater. Interfaces 2 (2010) 2254–2260.

[14] G.H. Kim, H.K. Song, J.Y. Kim, the effect of introducing a buffer layer to polymer solar cells on cell efficiency, Sol. Energy Mater. Sol. Cells 95 (2011) 1119–1122.

[15] G. Perrier, R. de Bettignies, S. Berson, N. Lemaitre, S. Guillerez, Impedance spectrometry of standard and inverted P3HT:PCBM organic solar cells, Sol. Energy Mater. Sol. Cells 101 (2012) 210–266.

[16] A. Mani, C. Huisman, A. Goossens, J. Schoonman, Mott–Schottky analysis and impedance spectroscopy of TiO$_2$/6T and ZnO/6T devices, J. Phys. Chem. B112 (2008) 10086–10091.

[17] G. García-Belmonte, A. Guerrero, J. Bisquert, Elucidating operating modes of bulk-heterojunction solar cells from impedance spectroscopy analysis, Phys. Chem. Lett. 4 (2013) 877–886.

[18] T.S. van der Poll, J.A. Love, T-Q Nguyen, G.C. Bazan, Non-basic high-performance molecules for solution-processed organic solar cells, Adv. Mater. 24 (2012) 3646–3649.

[19] C.J. Brabec, A. Cravino, D. Meissner, N.S. Sariciftci, T. Fromherz, M.T. Rispens, L. Sanchez, J.C. Hummelen, Origin of the open circuit voltage of plastic solar cells, Adv. Funct. Mater. 11 (2001) 374–380.

[20] M.C. Scharber, D. Mühlbacher, M. Koppe, P. Denk, C. Waldauf, A.J. Heeger, C.J. Brabec, Design rules for donors in bulk-heterojunction solar cells—towards 10% energy-conversion efficiency, Adv. Mater. 18 (2006) 789–794.

[21] G. Dennler, A.J. Mozer, G. Juška, A. Pivrikas, R. Österbacka, A. Fuchsbauer, N.S. Sariciftci, Charge carrier mobility and lifetime versus composition of conjugated polymer/fullerene bulk-heterojunction solar cells, Org. Electron. 7 (2006) 229–234.

[22] J. Bisquert, I. Mora-Sero, F. Fabregat-Santiago, Diffusion–recombination impedance model for solar cells with disorder and nonlinear recombination, Chem. Electro. Chem. (2013) (Published online).

[23] A. Guerrero, L.F. Marchesi, P.P. Boix, J. Bisquert, G. García-Belmonte, Recombination in organic bulk heterojunction solar cells: small dependence of interfacial charge transfer kinetics on fullerene affinity, J. Phys. Chem. Lett. 3 (2012) 1386–1392.

[24] C.J. Brabec, S.E. Shaheen, T. Fromherz, F. Padinger, J.C. Hummelen, A. Dhanabalan, R.A.J. Janssen, N.S. Sariciftci, Organic photovoltaic devices produced from conjugated polymer/methanofullerene bulk heterojunctions, Synth. Metals 121 (2001) 1517–1520.